

1/2U low-cost laser guide star payload

Ariel Sandberg,^a Albert Thieu^{ORCID},^{a,b} Anil Mankame,^a Zachary Palmer,^a
Joel Kiers^{ORCID},^a Mark Wilder,^a and Lulu Liu^{a,*}

^aMIT Lincoln Laboratory, Lexington, Massachusetts, United States

^bMassachusetts Institute of Technology, Space Telecommunications, Astronomy, and Radiation
Laboratory, Department of Aeronautics and Astronautics, Massachusetts, Cambridge,
United States

Abstract. We present all aspects of the development of a 1/2U laser guide star CubeSat payload. The payload, *AMS Beacon*, was integrated into the Agile Microsat (AMS) 6U platform developed by MIT Lincoln Laboratory and will function as a space-based point source reference for high-angle-rate adaptive optics (AO) control. In addition to a 500-mW onboard laser, it carries a retro-reflector and a photodiode (PD) with a 1 kHz readout. The system, launched successfully in May 2022 into low-Earth orbit, utilizes commercial components, fixed optics, and high-precision body-pointing enabled by a bus-provided GPS receiver, among other innovations, to keep the design compact and the costs low. To our knowledge, it is the first payload to be built as a test platform for high-angle-rate AO on orbital targets. The system architecture offers opportunities for future cost reductions and a strong foundation for payload proliferation across multiple satellites. The capabilities of the host spacecraft combined with the Beacon payload can also serve as a roadmap for integrating thrusting capabilities with an artificial guidestar, which would be critical in enabling various astronomical applications. © *The Authors. Published by SPIE under a Creative Commons Attribution 4.0 International License. Distribution or reproduction of this work in whole or in part requires full attribution of the original publication, including its DOI.* [DOI: [10.1117/1.JATIS.8.3.039003](https://doi.org/10.1117/1.JATIS.8.3.039003)]

Keywords: adaptive optics; guidestar; CubeSat; spacecraft; laser; payload.

Paper 22030G received Mar. 9, 2022; accepted for publication Aug. 3, 2022; published online Aug. 13, 2022.

1 Background

Historically, interest in putting a laser into space has primarily focused on the optical communications cross-link application;¹⁻⁷ however, a not-yet-flown class of proposals uses satellite-borne lasers as photometric calibration sources⁸ or laser guide star references⁹⁻¹² for high-precision ground- and space-based instruments. These systems are considered to be low-cost, agile “partners” to these expensive, high-sensitivity systems, and recognition of their potential is growing.¹³

Our interest lies in the domain of passive observation and active illumination of fast-moving space objects,¹⁴ aiding in general space situational awareness (SSA)¹⁵ including low-earth-orbit (LEO) debris classification and removal.^{16,17} For this application space, we have designed a miniaturized payload carrying a laser, a photodiode (PD), and a retroreflector. The laser acts as a point reference for optimization of an adaptive optics (AO) system on a fast-tracking telescope. This AO system is ground-based and may be active (equipped with a laser transmitter for illuminating the target) or passive (which we define as nontransmitting). For the subset of actively illuminating ground-based systems, the scoring PD provides feedback in the form of time-tagged power-in-bucket measurement, critical for calibrating such instruments. The retro-reflector enables the small payload to mimic a larger, noncooperative orbital target and is useful for tracking and ranging experiments.

In the 1990s, experiments in this space utilized high-cost, high-complexity, dedicated satellites including the Low-power Atmospheric Compensation Experiment (LACE) mission with its extensible 150 ft boom.^{18,19} More recently, designs in this space have evolved toward a more compact CubeSat form-factor,^{12,13} as the proliferation of available CubeSat commercial components has drastically reduced small satellite development timelines and costs. Our team targets an

*Address all correspondence to Lulu Liu, lulu.liu@ll.mit.edu

even smaller, ultracompact CubeSat payload form-factor, sporting the functionalities mentioned above. By opting for miniaturization and outsourcing our communications, attitude control, and power systems to a multitasking bus carrying multiple science payloads, we trade independence for development cost and a large number of mission opportunities.

Strategic design decisions and simplifications were made to achieve our SWaP (size, weight, and power) and cost targets. We minimized free-space optics, which are typically bulky and come with significant design and alignment overheads. We traded mechanical actuators and feedback control systems, typical of prior art missions in the domain of optical communication,²⁰ in favor of a generous beam divergence (~ 1.3 deg $1/e^2$ diameter) on a fully static, open-loop body-pointed system. These design choices compacted our payload to a $<1/2$ U, <300 g form-factor, which, by carrying nearly all commercial off-the-shelf (COTS) components, cost roughly \$300 k total to design and fabricate, including labor and integration but excluding launch.

Our application shares much in common with certain proposed astronomical surveys. As such, our design has the potential to dovetail nicely into the astronomical application space. For instance, Douglas et al.,²¹ recently proposed a formation-flying laser guide star secondary satellite for the Large Ultraviolet Optical Infrared Surveyor (LUVOIR) space telescope, which would enable the precision wavefront control necessary for high-contrast exoplanet imaging. This and other astronomical applications typically require stand-off distances much larger than the LEO range. To this end, our laser may be replaced with one that has higher power and lower beam divergence, and our PD may be replaced with a position sensing detector to track a reference beam from the ground. The retroreflector may help the imaging instrument “find” its spacecraft companion before the laser pointing is established, and our 1/2-U payload could be integrated into a more capable space platform with upgraded thrust and pointing capabilities and improved durability as needed for its particular mission.

2 Overview

2.1 Payload and Mission

The Agile Microsat (AMS) Beacon payload, shown in Figs. 1 and 2, is meant to establish flight heritage for on-orbit laser guide stars and to function as a multiuse testbed for high-angle-rate tracking, acquisition, and imaging applications compatible with a wide range of ground-based systems. As designed, it has three modes of operation: *passive mode*, in which the spacecraft points the beacon retroreflector toward the target; *down-link mode*, in which the beacon activates its on-board laser diode; and *cross-link mode*, in which the beacon activates both its laser and an on-board PD to measure received power at a 1 kHz readout rate. The high-intensity laser-diode (Tx) will provide a point-source phase reference for ground-based AO development and testing;

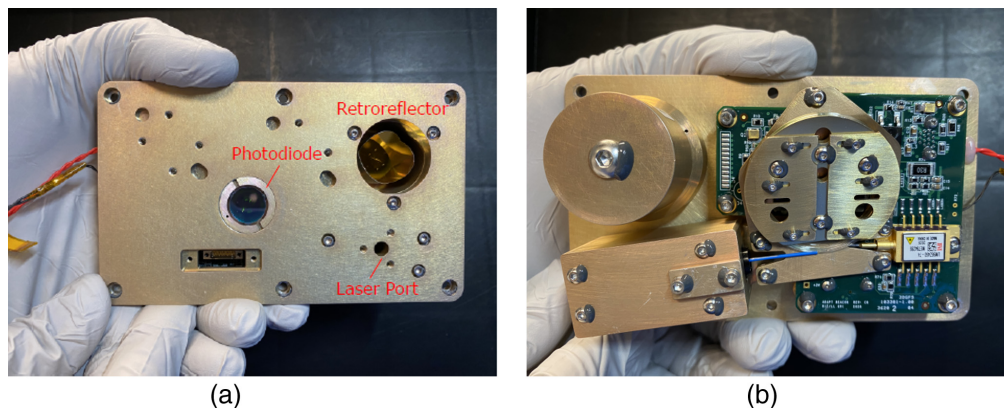


Fig. 1 AMS Beacon payload. (a) Payload exterior view. Laser port, ground support equipment (GSE) port, gold-coated hollow retroreflector, and PD optical stack visible. (b) Payload interior view. Optical paths mutually isolated and fully enclosed to minimize cross-talk and stray light.

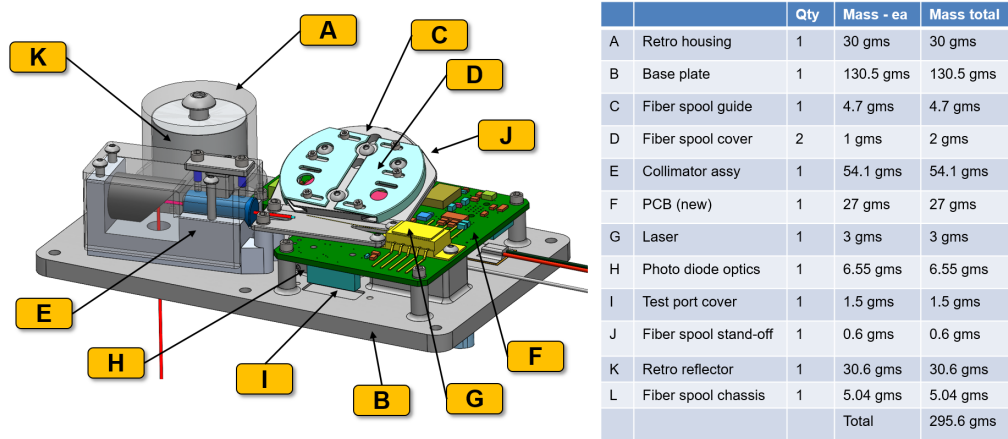


Fig. 2 AMS Beacon payload Solidworks model. Contains mass breakdown for each component. Weight estimate includes fasteners and mechanical hardware.

the on-board photodiode (Rx) will enable measurement of received optical power on-orbit for validation of the pointing accuracy and coherence of active illumination systems; and finally, the retroreflector will simulate a passive object reflecting incident light, progressing ground-based systems toward compatibility with noncooperative targets.

The payload is one of three on AMS,²² a mission funded internally by MIT Lincoln Laboratory and launched in May 2022 on transporter 5. The AMS mission deployed into a circular 500 km LEO sun-synchronous orbit. Over the course of its 6-month mission, the satellite will maneuver and perform a controlled descent. These maneuvers will be achieved through the use of an on-board field emission electric propulsion system and a novel flight control system for autonomously deriving and executing schedules for descent and altitude maintenance.

The mission is architected as a 6U CubeSat, see Fig. 3, with a total vehicle mass of roughly 12 kg and power production capabilities of 120 W. The vehicle will contain a suite of sensors and actuators for guidance, navigation, and control that will enable a nonthrusting body-pointing

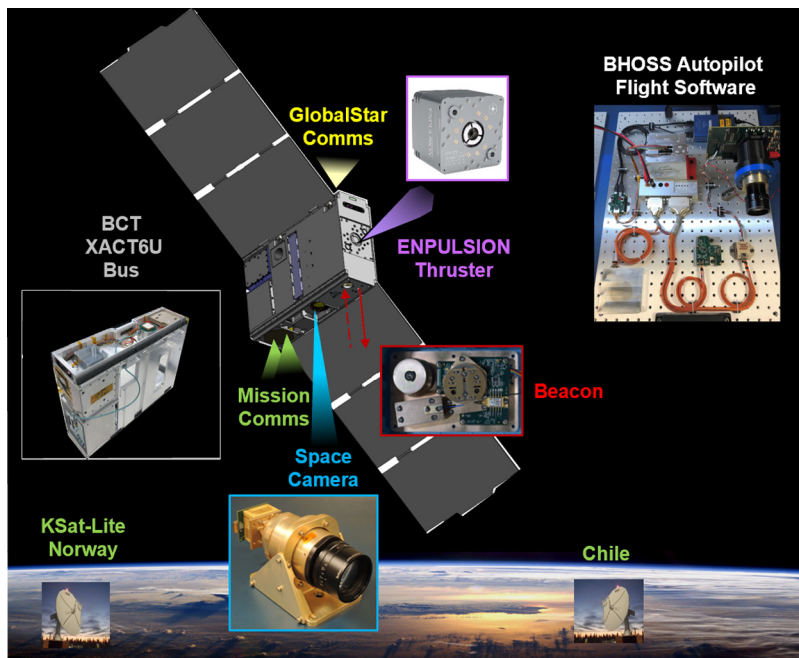


Fig. 3 Overview of 6U CubeSat AMS. AMS utilizes a COTS bus from Blue Canyon Technologies and carries three experimental payloads: a field emission electric propulsion ENPULSION thruster, a novel imaging camera, and the Beacon module.

accuracy of better than 0.1 deg, including a NovAtel OEM719 GPS (L1/L2) with 1.2-m positional accuracy.

Operation of the AMS Beacon payload is deconflicted from operation of the other two payloads (camera and thruster). In addition, for the duration of the space-to-ground link (usually about 100 s per pass), other than the attitude determination and control system (ADCS), all other sources of major electrical and mechanical interference will be shut off. The Beacon science mission is scheduled to begin early at the start of the AMS mission and resume periodically as schedule permits at lower orbital altitudes.

2.2 Concept of Operations (CONOPS) and Link Budget

During the Beacon science phase of the AMS mission, the laser will be operated during astronomical twilight or night to reduce competition from sky background. Due to our compressed development timeline, the optical ground station will not be equipped with any active illumination capabilities. We will be targeting validation of the payload down-link only during this first short-duration mission.

Engagements with the ground station (located at MIT Haystack Observatory) will occur above a minimum elevation angle of 40 deg, corresponding to a range of around 700 km. Thus, around 12 passes will be available per month during the expected AMS mission timeline based on an initial 500-km sun synchronous orbit, with these passes spread relatively evenly across the month. Each pass has an average duration of 102 s above the minimum elevation angle. Approximately 5 min before the time of closest approach (TCA), the AMS satellite will point the Beacon laser at the ground station in Earth-centered Earth-fixed frame. At 2.5 min before TCA, the laser will turn on to a stable, full-power state outputting ~450-mW optical power. The laser will then remain on until 2.5 min after TCA. AMS will then return to its previous attitude configuration following the laser firing. The full sequence is depicted in Fig. 4. Based on systems tool kit models, these pass opportunities will occur no more than once per night for a maximum of three nights in a row, followed by multiple nights with no viable passes. This expected duty cycle and laser firing duration are well within Beacon payload power budgeting for AMS and thermal limits for the Beacon hardware itself. Beyond standard operations, the laser will also be selectively operated during active thrust phases of AMS with a secondary science objective of assessing the Beacon’s capability during active, low-impulse thrust maneuvering.

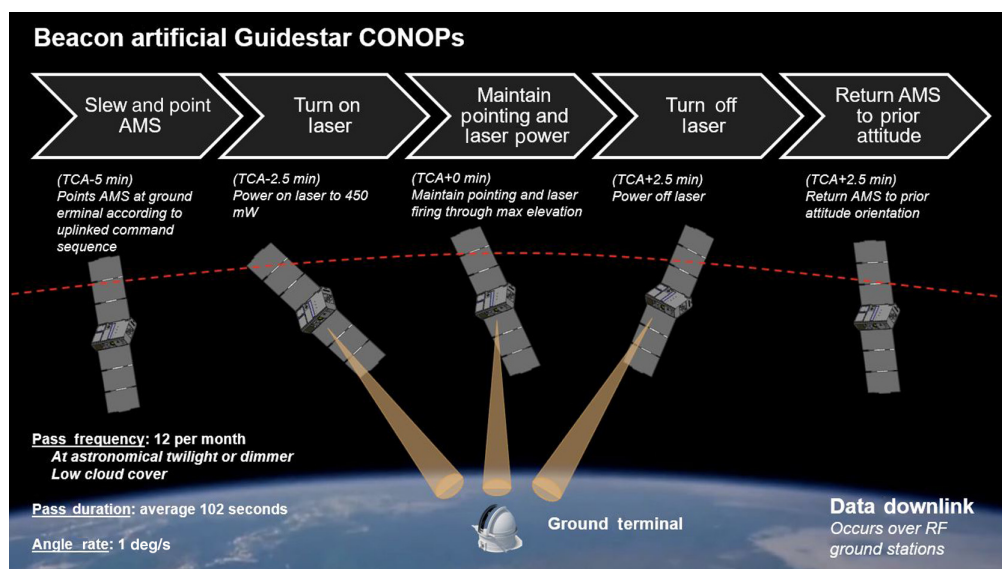


Fig. 4 Beacon CONOPS. Command sequence during single AMS Beacon pass over optical ground terminal.

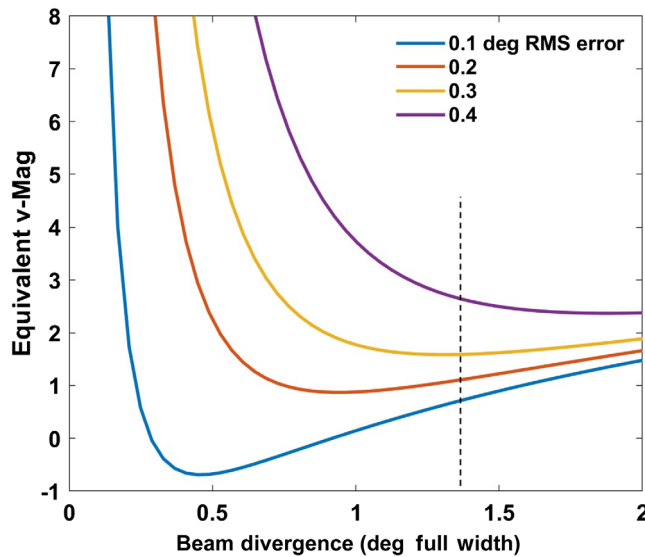


Fig. 5 Beam divergence optimization. 10-percentile estimated photon flux at ground station as a function of $1/e^2$ beam divergence and normally-distributed root-mean-squared (RMS) pointing error. Dotted line shows design point. Nominal pointing error specified by vendor equals 0.1 deg.

Figure 5 shows the space-to-ground downlink analysis, which set our desired beam divergence to 1.3 deg, based on a pointing accuracy specified by the vendor of about 0.1 deg. To incorporate robustness against larger than expected deviations, RMS pointing errors from 0.1 to 0.4 deg were considered. With a final ground system design still pending, we chose to express our flux in equivalent apparent magnitudes over the visible band, which is expected to be between -1 and 3 , depending on the ultimate error stack-up. A v -Mag of -1 is equal to the brightest star in the sky.

3 Beacon Payload Development

3.1 Design

The Beacon payload was designed to support the three operational modes discussed in Section 2.1. Additional drivers during payload development included minimizing impacts to the host spacecraft by maintaining a low SWaP design, as well as promoting interoperability with potential future hosted missions by maintaining a simple interface in both electrical and mechanical terms. To this end, the payload as designed and assembled requires of the host satellite a single 5 V power rail, an RS-422 command and telemetry link, body pointing as discussed in Section 2.1, and thermal control in the form of maintaining the payload within a specified operational temperature range while accepting waste heat from the payload. A single circuit board roughly $7\text{ cm} \times 6\text{ cm}$ in size contains all of the payload electronics. The payload consumes $<2.0\text{ W}$ when the laser is active and $<200\text{ mW}$ otherwise.

The payload consists of four major subsystems as shown in Fig. 6: processing, receive, transmit, and retroreflector. The processing subsystem handles commands, controls and monitors the receive and transmit subsystems, and creates telemetry packets to send to the ground. The receive and transmit subsystems are built around the needs of the primary PD and laser, respectively. Finally, the retroreflector required for the passive mode of operation can be viewed as a stand-alone subsystem with no electrical dependencies.

The transmit subsystem is built around a fiber-coupled, passively cooled diode laser (II-VI UM96Z460-76). The maximum output power is 450 mW, and the wavelength is 976 nm with a center wavelength drift of $<0.5\text{ nm}$ over the full operating temperature range of 0°C to 45°C . The center wavelength was a compromise among a multitude of considerations, primarily, relaxed complexity of AO systems at longer wavelengths, total atmospheric transmission, cost

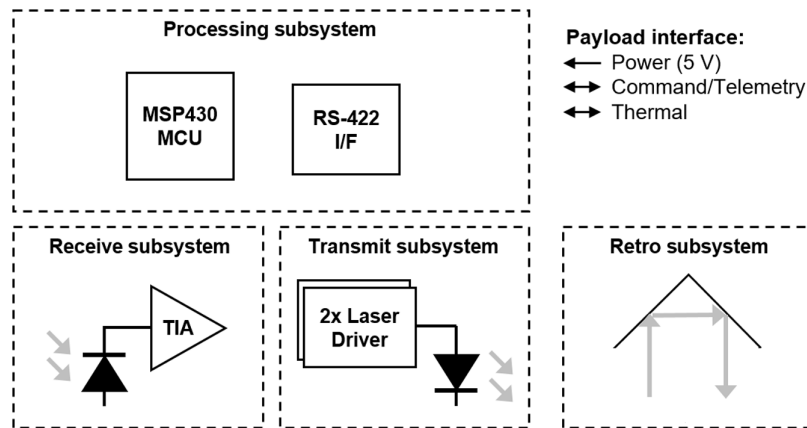


Fig. 6 Beacon system diagram. Functionality of Beacon payload comprised of four key subsystems: processing, receive, transmit, and retroreflector. Interface of payload intentionally kept as simple as possible.

of ground-station sensor technology, and ease of exclusion of sky-background. To keep the design simple, compact, and low-power, the laser diode relies on passively conducting heat to the payload baseplate for cooling instead of utilizing a thermoelectric cooler (TEC). The peak power is a compromise between the heatsinking capability of AMS, the availability of moderate-to-high powered pigtailed laser diodes, and the needs of the link budget presented in Sec. 2.2.

The selection of a pig-tailed laser kept the design simple and compact by eliminating many free-space optomechanical components from the payload design and consequently reducing the need for tight tolerances and complex alignment steps during assembly. Supported by high-precision body-pointing offered by the host satellite attitude determination and control system, we chose a beam divergence of 1.3 deg ($1/e^2$ diameter) based on the link optimization described in Sec. 2.2. An optical fiber splice joined the laser with a pig-tailed collimator (Oz Optics LPC-04-980-6) that was customized to produce this divergence.

Though selecting a pig-tailed laser kept the optomechanical design simple, it did introduce the complication of fiber management. The position of a fiber Bragg grating (FBG), which stabilizes the wavelength of the laser output, placed a minimum length constraint of about 0.8 m on the optical fiber that had to be stowed in the payload. We utilized a custom-designed and fabricated spool for winding the fiber into a compact coil, which was then secured with a sliding cover. As the fiber assembly contains a very fragile configuration—a diode laser on one end, a collimator on the other, and a fiber joint in the middle (see Fig. 7)—the fiber coiling operation was completed with great care on a separate winding fixture to minimize risk of handling damage. The assembly was mounted to the payload baseplate and stabilized mechanically using

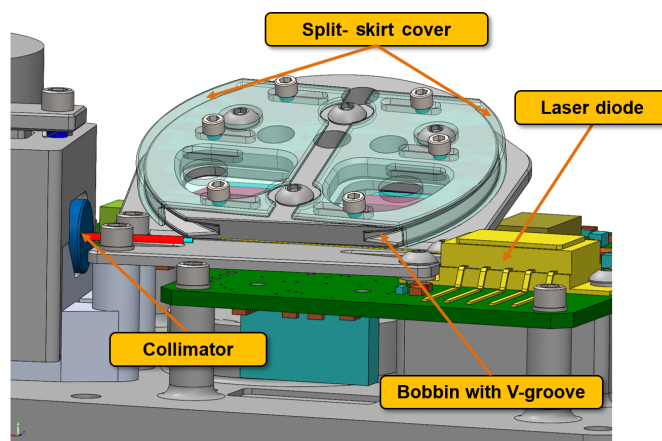


Fig. 7 Mechanical details of fiber spool assembly.

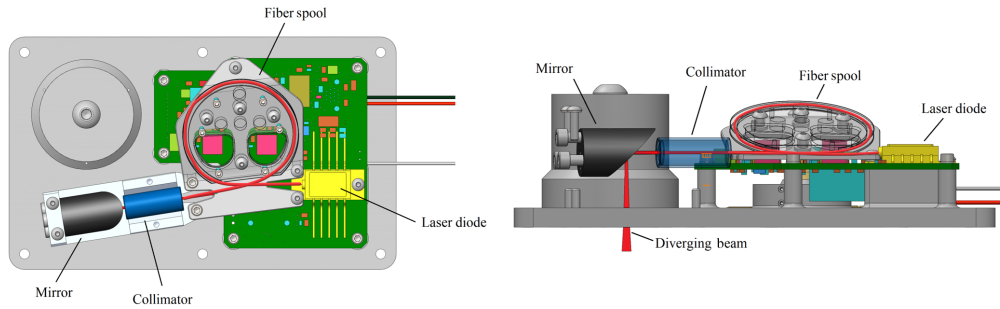


Fig. 8 Beacon payload transmitting optical path. Majority of the optical path is in-fiber, with the only free-space portions downstream of the collimator. This design was chosen for maximum thermal and mechanical pointing stability.

stand-offs so that it did not interfere with elements on the printed circuit board (PCB) underneath while achieving a compact form factor for the payload (Fig. 8).

The fiber assembly consists of a V-grooved bobbin and a set of split skirts. The diameter of the spool and the size of the V-groove were optimized to package the fiber in its most efficient space-saving configuration without compromising the minimum bend-radius requirements. The split skirts were designed to gently nudge the fiber coil into the V-groove such that the fibers were secure and positively captured for safe accommodation of launch loads. This subassembly was then transferred back to the baseplate to be mounted. The spool was fastened to its stand-offs, the collimator clamped into an enclosed optical fixture with a 45 deg fold mirror for directing the beam into space, and the laser diode soldered onto the PCB (see Fig. 9) with a sandwiched graphite thermal interface layer to facilitate heat dissipation into the baseplate .

The power conditioning for the laser diode is handled by a constant-current buck regulator (TI TPS92513). This laser driver supports the dimming of the laser over a 10:1 dynamic range, controllable via ground command; critically, this dimming is implemented via modification of the regulator set current instead of pulse width modulation (PWM) control, so a high-frequency ripple in the laser output is avoided. This functionality compensates for the laser’s narrow operating temperature range by providing for a low-power prewarm mode. As the laser power conditioning circuit is built with commercial-grade components, two fully redundant copies of the power conditioning circuitry were incorporated in the payload PCB to enhance reliability.

The transmit subsystem also includes a laser lockout function for use during ground testing. Given the high output power and near-IR (NIR) wavelength of the laser diode, a reliable method of ensuring that the laser was inactive was necessary to promote personnel safety. The lockout

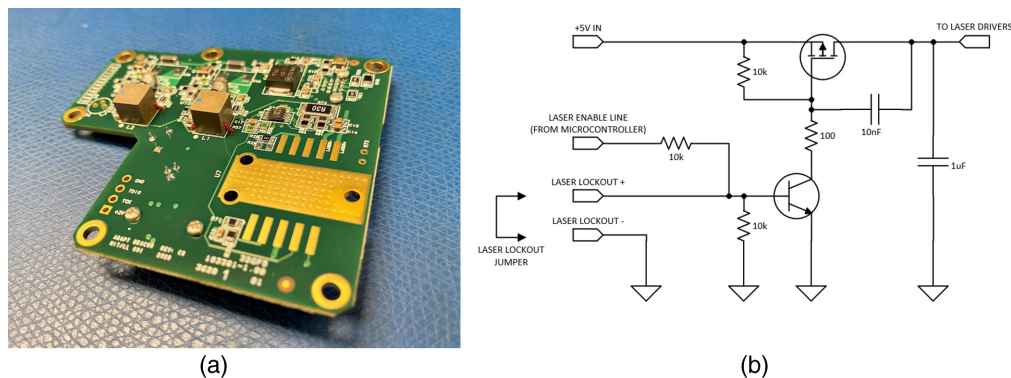


Fig. 9 PCB details. (a) Top surface of PCB. Top-left corner features two redundant laser drivers. Bottom-right corner contains footprint for laser diode, with array of thermal vias to conduct heat to bottom surface, which contacts payload baseplate. (b) Schematic of laser lockout circuit. Externally connecting two pins on payload’s test connector overrides microcontroller’s control authority and disables load switch to ensure that lasers are de-energized regardless of commanded state.

functionality of the payload prevents the laser drivers from activating when a set of two pins on the payload debug connector are shorted together. During ground testing of the payload, we used a custom high-visibility lockout plug as an element in our laser safety plan. After ground testing was complete, a nonshorting aluminum connector cover was installed to prevent accidental activation of the lockout function while on-orbit.

The receive subsystem, which is required for the cross-link mode in the CONOPS, is built around a PD. We selected an InGaAs PD with a large active area (Thorlabs FGA21) for this purpose; it is mounted on the payload PCB. In front of the PD, an optical tube contains a 1064 ± 5 nm bandpass filter (modified Thorlabs FL051064-10) to isolate the expected signal from Earth's albedo, as well as a coated asphere lens (Thorlabs 352240-1064) to concentrate light onto the PD's active area. The selection of a PD with a large active area ensured that precise alignment of the optical stack to the PD was not required, easing assembly. The PD must detect signals attenuated by spreading loss and atmospheric absorption at the relatively low rate of 1 kHz; given the low bandwidth required and the need for low noise measurement, the PD is biased in photovoltaic mode instead of photoconductive mode. A low-noise transimpedance amplifier converts the photocurrent to a voltage, which is then read by the payload microprocessor with an integrated analog-to-digital converter (ADC). The ADC noise dominates the link budget.

The passive mode of operation in the CONOPS requires a retroreflector subsystem. We selected a compact hollow aluminum, gold-plated retroreflector (Newport Optics 50326-1002) for this payload. The diameter of the clear aperture of the retroreflector (~ 19 mm) was chosen to be as large as possible while accommodating an expected point-ahead angle of ~ 50 μ rad, as is typical for most LEO targets. As such, the minimum coherent spot size on the ground is expected to be about 30 m in radius, larger than the expected offset due to finite light round-trip time (around 25 m) and eliminating the need for any costly custom process for *spoiling* the returns from the retroreflector.

The payload electronics incorporate redundancy and fault detection to improve reliability and mitigate the expected radiation environment. The short mission duration coupled with a low orbit and 0.2" aluminum shielding ensure that the total ionizing dose (TID) that the payload will experience is on the order of 100 rad(Si) (Computed using SPENVIS data²³); this low TID justifies our use of low-cost, commercially-available components in the payload, but the potential remains for damage caused by single event latch-up (SEL) due to energetic particles. Additionally, it was desirable to design a payload that could be included on future missions with more challenging radiation environments. To address this concern and improve reliability, the payload utilizes a radiation-hardened microprocessor that is immune to SEL up to a linear energy transfer (LET) of 72 MeV-cm²/mg (TI MSP430FR5969-SP) for the core functionality of the processing subsystem. Identified as another potential single point of failure, all communication with the host satellite is handled via another radiation-hardened chip, a RS-422 transceiver (TI SN65C1168E-SEP); this ensures that the payload remains responsive to the host satellite and/or ground control.

The processing subsystem monitors key temperatures in the payload and disables other subsystems if high/low temperature limits are exceeded. It further monitors the current in the power regulation circuits; upon detection of the abnormally high currents that are indicative of a latch-up event, the mission software hosted on the microprocessor automatically resets the affected subsystem to prevent damage from thermal runaway. These design decisions and the inclusion of redundant power conditioning circuits for the laser diode position the Beacon payload to perform well both on the AMS mission as well as on any potential follow-on missions (Fig. 10).

3.2 Environmental Testing Highlights

The testing methodology for AMS Beacon involved the initial evaluation and risk reduction testing of components without space heritage, before advancing to system-level testing of an engineering model payload to NASA General Environmental Verification Standard (GEVS) qualification levels.

The most notable COTS component without flight heritage was the fiber-coupled laser diode. The laser unit presented several major risks: the fiber coating and strain-relieving boot had the

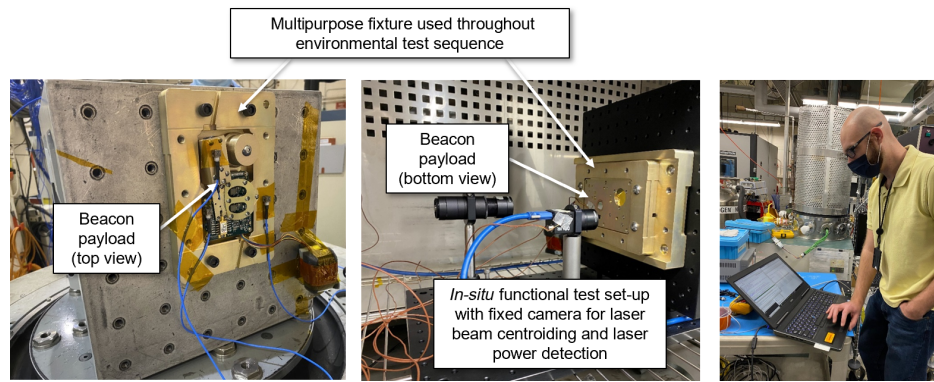


Fig. 10 (a) Environmental test configurations. Unpowered three-axis random vibration testing to qualification levels, maximum predicted environment (MPE) $+6$ dB = 13.84 G_{rms} , 20 to 2 kHz. (b) Thermal testing with *in situ* beam characterization and alignment verification over a temperature range of 0 deg to $+50$ deg. (c) Vacuum testing with laser performance monitoring at a pressure of 5.0×10^{-5} Torr.

potential to outgas in vacuum; the solder interface joining the laser diode leads to the PCB contacts was required to withstand significant launch loads and moderate thermal loads; the attached fibers were delicate and needed to be held by a specially designed strain-minimizing fixture; and finally, the laser package itself had to be qualified in vacuum for hermeticity and structural soundness.

After an initial vacuum bake-out test showed high levels of outgassing from the unmodified laser package, a delicate procedure was undertaken to remove the rubber strain-relieving boot without damaging the fiber that it protected. The boot was sliced open length-wise, and a technician peered beneath it for evidence of epoxy. When no epoxy was discovered, the boot was pulled away from the laser housing with tweezers. A repeat vacuum bake-out test confirmed the successful removal of the source of outgassing.

To address the survivability of soldered interfaces and thermal performance under continuous operation, a mechanical finite element model (FEM) was created to predict loads at board interfaces based on a preliminary design, and a steady state thermal model was created to ensure that temperatures during operation fell within safe operating limits. The structural analysis revealed potential failure locations, which led to a redesign of the PCB to incorporate additional points of support. The laser diode leads (see Fig. 7) were also reformed with these structural loads in mind. These modifications led to a more robust design that was validated with additional simulations (see Fig. 11) and vibration testing. The parallel investigation into the thermal viability of the laser and fiber from self-induced heating showed insignificant impact due to the fact that the sub-structure's thermal mass was significantly larger than necessary. Also, the only free-space optical path in the system, located in the vicinity of the collimator and the folding mirror assembly, was sufficiently far enough from the heat source that it was deemed a nonfactor for any additional thermal analysis. This was later corroborated by the thermal chamber tests, which showed that the resultant distortions were within the anticipated error budgets.

The COTS laser package was not designed with vacuum applications in mind, and a true in-house hermiticity test was out-of-scope for our program. Instead, we devised a powered vacuum test of the unit, during which a functional test script monitored several metrics of laser performance and compared their values at the start and end of a 24-h period in high-vacuum (10^{-5} Torr). These metrics were laser current draw, steady-state operating temperature, and output optical power as measured by a PD built into the laser package. In addition, the script checked the payload software compliance and validated performance of the high-rate PD data-stream, the software safety limits, and the communication protocol. As shown in Fig. 12, no deviations in laser parameters were observed in our vacuum test. Coupled with the manufacturer's qualification testing data, which measured a leak rate under 1×10^{-10} atm-cc/s on 12 sample devices after damp heat and high temperature storage, we felt that the risk had been adequately mitigated for our 6 month mission.

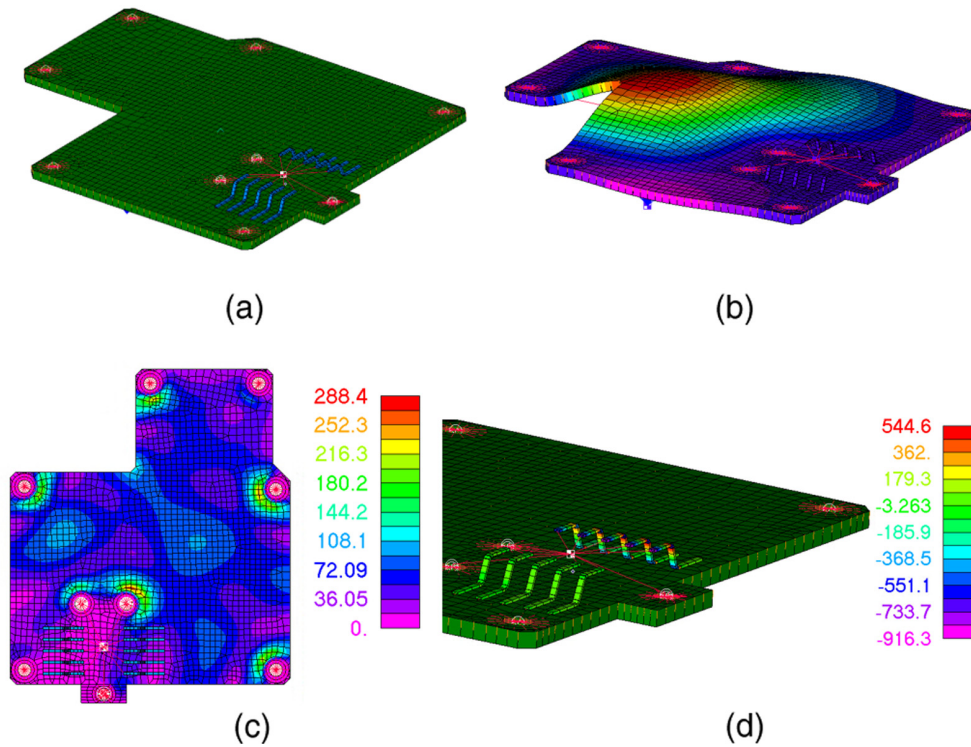


Fig. 11 PCB structural analyses—results. (a) Structural constraints, (b) analysis shows the PCB’s first vibrational mode to be ~2108 Hz, which is greater than the highest frequency in the test spectrum (NASA GEVS), and hence no fatigue analysis was deemed necessary, (c) calculated max stress in PCB (psi), $\sigma_{\text{allowed}} = 30$ ksi, (1 ksi = 1000 psi), and (d) calculated max stress in laser lead wires (psi), $\sigma_{\text{allowed}} > 30$ ksi.

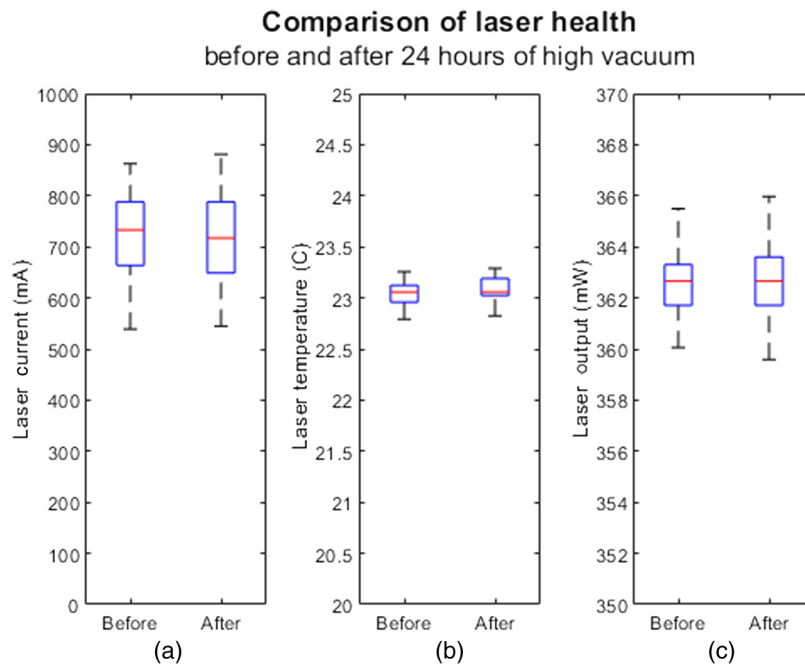


Fig. 12 24-h high-vacuum laser qualification test. Laser health compared along several dimensions at start and end of 24-h period under high-vacuum conditions. Box plots indicate quartiles of parameters over 2 min of observation after laser has thermalized to environment. No degradation observed—laser output power remained unchanged for a similar input current, and temperature indicated no excess heating of the laser.

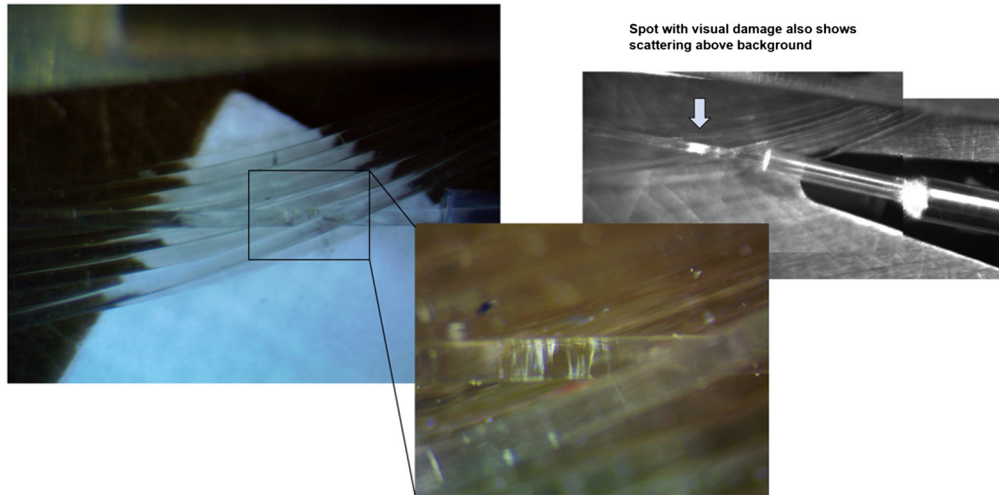


Fig. 13 Damaged area on fiber cladding. (a) Damaged region under white light illumination. (b) Same region with laser powered on.

At one point, a visual fiber inspection after laser burn-in revealed damage to the fiber coating, with the damage potentially reaching down to the fiber cladding. A close-up of this area is shown in Fig. 13. A root cause investigation revealed that the damage most likely occurred during boot removal, and determining that the risk of deintegrating the existing unit was lower than that of potentially flying a damaged laser, the laser was replaced with a spare. Once installed, this spare laser passed subsequent inspection. Because the anomaly was observed after system integration but prior to initiating the environmental test campaign, the test campaign was able to proceed as planned with no regression testing required.

Beyond the component level, all payload scientific objectives hinged on the ability to maintain our laser beam alignment relative to fiducials on the spacecraft. For our gimbal-free body-pointing strategy to be effective, the laser alignment needed to be precisely measured relative to the vehicle star trackers, and the free-space optical path had to be stable throughout the range of on-orbit environments. Using a fiber-coupled laser, we intended to minimize the free-space components within our payload. Only two optomechanical components had the potential for thermal drift: the assembly holding the fiber collimator and the 45° turn mirror. We monitored the stability of these components by measuring the beam alignment relative to fiducials before and after each system-level environmental test, as shown in Fig. 14. During thermal cycling, the alignment was measured *in situ* to capture drifts at temperature (see Fig. 15). For all environments, the beam displacement was found to be well within our 0.1 deg RMS requirement.

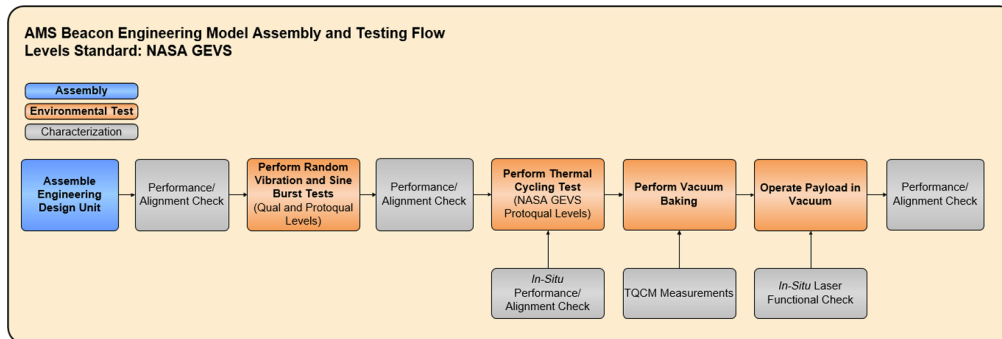


Fig. 14 AMS Beacon engineering model assembly and testing flow. Sequence of system-level environmental tests and characterizations that AMS Beacon engineering model underwent for system validation.

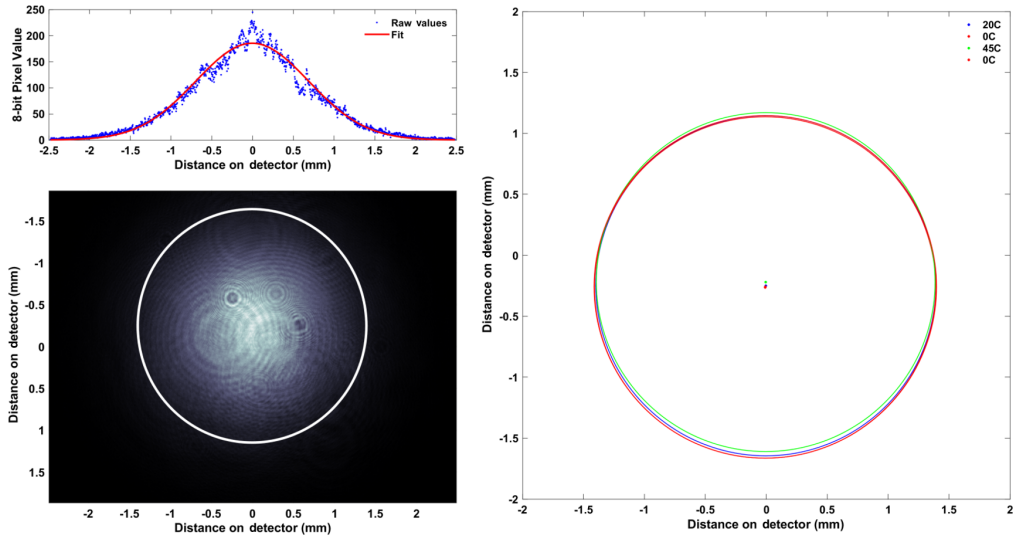


Fig. 15 Laser spot repeatability tests. (a) Image of Gaussian laser spot with $1.3^\circ 1/e^2$ beam divergence. $1/e^2$ diameter of 2D Gaussian fit shown overlaid with camera image. Cross-section of pixel values shown above the camera image along with the Gaussian fit. (b) Measurement of beam drift over operational thermal range (0 to 45C). Centroid and $1/e^2$ diameter of laser spot plotted for different oven temperatures. Distance between laser aperture and camera is fixed at 110 mm.

3.3 Laser Boresight Characterization

With no moving components, and without a reference signal from the ground to correct payload pointing in real time, the success of the Beacon downlink relies on a lab calibration of the laser boresight vector relative to a fixed spacecraft reference frame. However, the 6U bus offered by the vendor included no calibrated body-frame fiducials on the exterior of the spacecraft; in fact, the body axes of the spacecraft were defined in software only, and all spacecraft attitude maneuvers are referenced to the main star tracker (ST1). This complicated our alignment procedure as ST1 and Beacon payload were mounted on different faces of the bus (see Fig. 16), and both had to be characterized relative to the lab frame to be related to one another. Furthermore, because the roll of ST1 corresponded to the pitch of the Beacon laser, uncertainty in this quantity directly limited the precision of the calibration. Care was taken to develop a procedure that would address these challenges.

To find the boresight and roll of ST1, a Leica TM6100A theodolite (Hexagon AB) with autocollimation attachment was set up ~ 10 m in from and looking into ST1 (see “Theodolite Position 1”). With the theodolite focused at infinity, its autocollimation cross target was projected onto the ST1 imager. Image frames could then be stored and a MATLAB script used

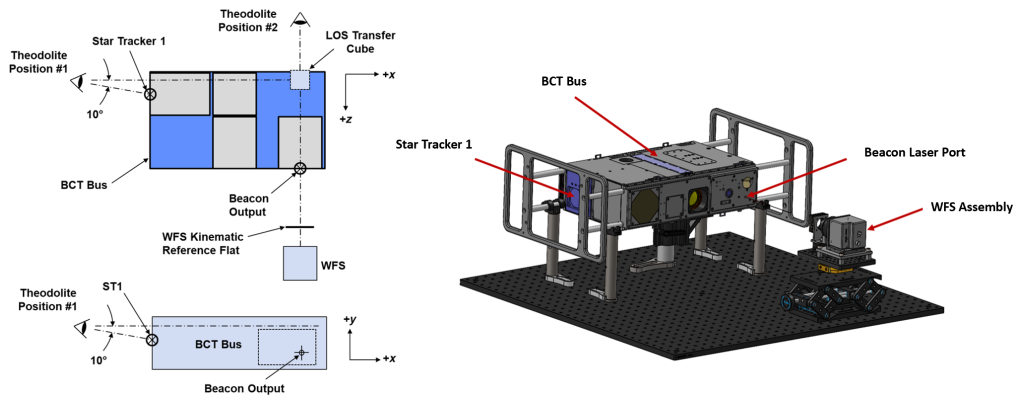


Fig. 16 Beacon alignment schematic and Solidworks mock-up. Note that the procedure utilizes only one theodolite, placed in two positions (labeled 1 and 2).

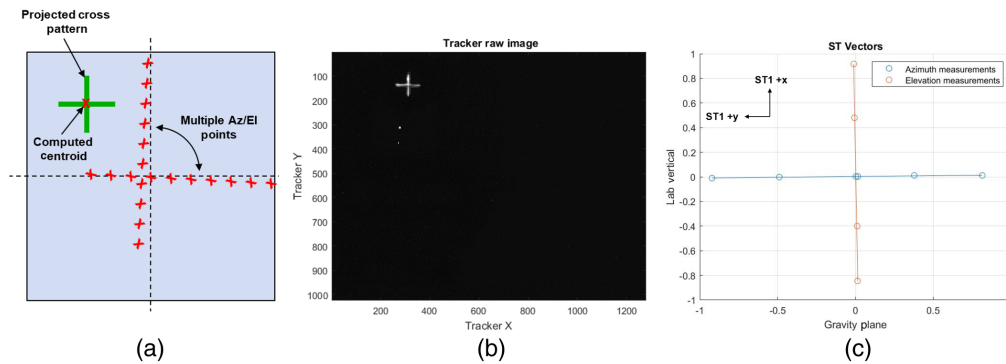


Fig. 17 Star tracker 1 roll measurement. (a) Schematic representation of cross image taken on ST1 and computed centroid. Multiple measurements used to compute ST1 roll relative to gravity vector. (b) Example raw image extracted from ST1, X- and Y-axes labeled in pixel space. (c) Acquired data from which the roll angle of 0.8 deg was computed.

in real time to determine the centroid of the cross image in the calibrated ST1 reference frame (see Fig. 17). Thus, the theodolite cross was centered on the ST1 normal (0,0,1) vector to <0.001 deg, and its azimuth (az) and elevation (el) were recorded. A series of points were then measured ± 2 deg from the center of the imager, in az (horizontal) and el (vertical). From this dataset, the roll of the ST1 imager, relative to a gravity plane, was computed.

To transfer the line-of-sight (LOS) from the ST1 face of the spacecraft to the orthogonal Beacon face of the spacecraft, we used a high-precision optical alignment cube. The mirrored faces of the cube were specified to be orthogonal to arc-second precision and thus facilitates precise 90-deg rotations in space.

The final challenge was to measure precisely the boresight of a diverging NIR beam. An Imagine Optics HASO3 wavefront sensor (WFS) was deployed for this purpose. With the Beacon laser operating at low power (~ 10 mW), the WFS was positioned a short distance away from the laser port such that the beam was centered on the collecting area of the device. The WFS could then be adjusted in tip/tilt to null the measured average tilt to better than 0.2 waves.

With the WFS representing the laser boresight and the alignment cube representing ST1 axes, we were able to move the theodolite to a position where it could sight both vectors and measure their angular deviation from one another. To check our characterization result, we used the ADCS definition of bus body axes relative to ST1 axes to compute our laser boresight result in the bus body frame. Finding this vector to be nearly normal to the z -face of the bus [-0.297 deg (x - z plane, azimuth) and -1.025 deg (y - z plane, elevation)], the result reflected our design intentions and was in rough agreement with lower fidelity measurements taken preintegration.

3.4 On-Orbit Risk Mitigation

The strategies described in Secs. 3.2 and 3.3 go a long way toward mitigating the risk of on-orbit pointing errors of our laser. Nevertheless, between beam characterization and launch, a number of events may change the relative orientation between the Beacon laser and ST1. We developed an attitude control sequence supported by ground radiometric analysis to be activated in case of a weak or nondetectable signal.²⁴ *Search Mode* slews the spacecraft in a predetermined pattern to locate the beam and update beam alignment, and *Optimization Mode* repeats a similar pattern over a smaller area with the objective of maximizing flux at the ground station.

Search mode calibration relies entirely on native spacecraft telemetry and optical ground station acquisition infrastructure. The aim of this mode of operation is to systematically slew over the widest ground area possible without holes or voids in the footprint. A link analysis of the laser beam footprint informed the effective diameter of the ground spot that would allow for detection of the laser by ground station sensors with a signal-to-noise ratio (SNR) of 6. These parameters were baselined for the range extremes of a typical pass, 700 km, while

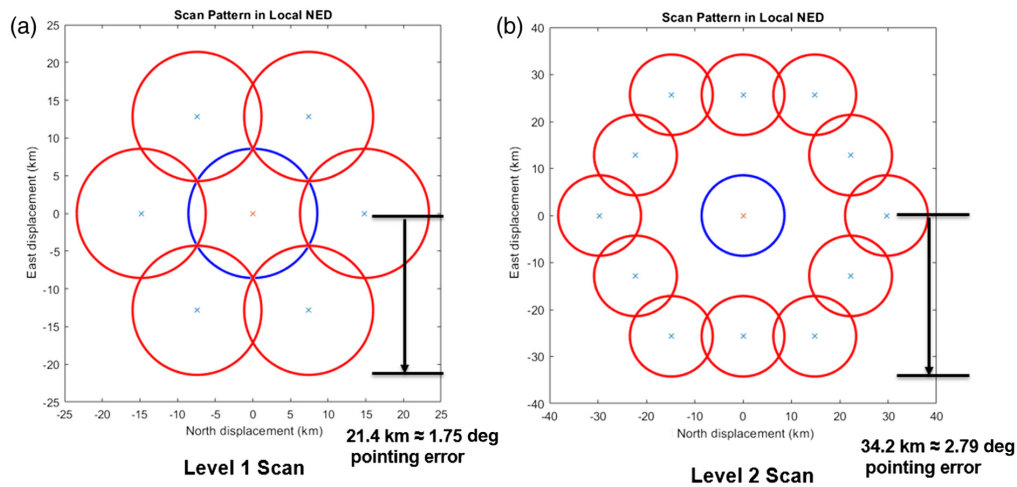


Fig. 18 Beacon search scan mode. (a) Level 1 search scan to cover immediate area around boresight geolocation (circle in red) over singular pass. (b) Level 2 search scan to cover area surrounding level 1 search scan if necessary.

operating the laser at the maximum 450-mW power. The beam footprint radius was estimated to be around 8.5 km under conservative atmospheric and camera sensitivity assumptions.

The scan sequence is constrained to operate within the slew capabilities of the satellite ADCS. The satellite ADCS is capable of slewing up to 5 deg/s but requires time to ramp up to this slew rate as well as time to settle on a ground target. Additionally, the satellite flight software does not contain any dedicated mode to slew the satellite in a smooth, nonlinear pattern such as a circle or spiral on the ground. Therefore, a two-dimensional (2D) hexagonal step-stare around the initial ground target was chosen. Figure 18 shows the ground area for a simulated search scan around the initial ground target, with AMS’s capabilities verified using a flatsat and dynamics processor setup that accurately simulate AMS attitude capability and Beacon laser firings. A level 1 hexagonal scan can cover a ground area with a radius of ~ 21.4 km, or about 1.75 deg. The scan can then be expanded to additional concentric rings for greater area coverage as necessary. For example, a level 2 scan extends the radius of the coverage zone to 34.2 km, or about 2.79 deg. Although the largest area covered during a single pass is limited by the spacecraft’s slew rate and settling time, by keeping the secondary pointing direction of the satellite consistent across passes, multiple scans across multiple passes can be concatenated to cover as large an area as necessary.²⁵

By combining radiometry data collected at the ground with time-stamped position and attitude data from the spacecraft and correlating the maximum intensities with associated spacecraft attitude, beam boresight (direction of maximum flux) can be derived. This process requires appropriate normalization of the radiometric intensity based on the satellite range. Similar on-orbit alignment calibration activities have been performed previously for laser communication satellites.¹

The Optimization Scan uses a similar pattern to the search scan but incorporates multiple levels during a single pass. The smaller scan will step-stare with an angular resolution of 0.1 deg spanning a 0.4 deg area, or a 3.2-km geographic extent at expected orbit altitudes. This procedure can also be executed independently of the search scan. The tighter scan allows for collection of radiometric intensity data at the ground station with a higher angular resolution, allowing for more precise determination of the laser’s true boresight.

4 Beacon as Model for Future Systems

AMS Beacon is a low-cost multifunctional optical link testbed consisting of a laser, PD, and retroreflector, which can be utilized as a base design for an optical communications terminal, an on-orbit guide star for AO, or a test target for ground-based tracking or illumination systems. Flying as a secondary payload on AMS, its success will provide an attractive, alternative

development architecture for active payloads as secondary payloads on CubeSat or small satellite missions, with operations interleaved with host satellite primary missions operations. It was developed as a ½U, <300 g payload to a 6U CubeSat, its miniature form-factor maximizing deployment opportunities and minimizing its costs of development. Though the system was developed over 2 years with a budget of around \$300 k, it can be duplicated with minor modifications for < \$50 k by leveraging COTS components that will gain heritage through this initial flight.

The low-cost, CubeSat-compatibility emphasis of the Beacon payload also provides a strong foundation for payload proliferation across multiple satellites. This can be useful in the context of optical communications or in its current capacity as a laser guidestar. A constellation would allow for more frequent engagement with select ground stations and better sky coverage.

Although the maneuverability of AMS will not be primarily used in support of Beacon laser operations, our ability to test the laser before, during, and after AMS thruster operations will demonstrate the capability to accurately point an on-orbit laser guidestar from a maneuverable CubeSat. Most proposed space-based laser guidestars for large-aperture telescopes rely on a maneuvering capability to allow the telescope to image different targets in sequence;¹² unfortunately, the degree to which precision pointing is compatible with satellite agility is not yet well understood. A laser beacon aboard a maneuvering CubeSat is also appealing for its flexibility to change its ground track to service different observatories on demand. The capabilities of the AMS host spacecraft combined with the Beacon payload will provide operational experience to inform both of these use cases and can serve as a roadmap for integrating thrusting capabilities with an artificial guidestar.

To actually adapt the system to astronomical applications, a prudent choice must be made for the satellite host and a set of modifications made to the payload itself. The host satellite requirements will depend on the specifics of the instrument that it is aiding and the class of science targets that it is imaging, but under most circumstances, a spacecraft with significant thrust capability will be needed to maneuver between targets. For a space-telescope, such as LUVOIR, additional thrust may be required for maintaining stability between the telescope and its LGS companion. On the other hand, for a ground-based telescope, the rotation of the earth is a major factor. The higher the apogee of the orbit, the lower the apparent motion between the laser guide star and any “fixed” astronomical science target. For an object in GEO, only a few seconds of integration time is available before the laser guide star exits the isoplanatic patch around the science target. However, our team has produced some models to suggest that special retrograde highly elliptical orbits can be designed that would enable integration times on the order of tens of minutes to an hour. Very likely, a dedicated launch would be required to take a spacecraft into such an orbit, and the higher costs involved will demand a longer mission life time and improved ruggedness of the bus.

Major modifications that must be made to our payload for an astronomical application are likely to include the laser power and/or laser beam divergence, the sensitivity of our detector and the number of pixels, and the introduction of radiation-hard electronics components. If stand-off distances exceed LEO ranges, our current beam design will not close the optical link. For instance, to recover the same link at GEO ranges, we must compensate for about a 70x increase in distance. This can be accomplished by shrinking the beam to a $1/e^2$ diameter of about 350 urad. Current ADCS systems coupled with onboard GPS receivers are capable of body pointing to that level of accuracy, but significant care must be taken to eliminate relative thermal shifts between the star-trackers and the laser boresight. One way of doing this might be to mount the star-trackers and the fiber launcher on a common Invar block. But most likely, to relax our pointing requirements, we will also want a more capable laser. Fiber lasers (in development at MIT Lincoln Lab among other institutions) have the capability to reach over 10 W through the insertion of amplification stages. On the other hand, open-loop pointing may not be an option for a space-telescope partner such as an LGS for LUVOIR due to the lack of fixed references. In such cases, closed-loop pointing may be activated by placing a beacon on the telescope and replacing the current 3 mm active area InGaAs PD with a position-sensitive detector with multiple pixels. The position signal can then be used in closed-loop with the ADCS to dial in the optimal pointing attitude. These additional capabilities will likely grow the SWaP of the payload, which will need to be traded against its proliferation potential.

Acknowledgments

This material was based upon work supported by the Under Secretary of Defense for Research and Engineering under Air Force Contract No. FA8702-15-D-0001 and the National Science Foundation Graduate Research Fellowship Program under Grant No. 1745302. Any opinions, findings, conclusions or recommendations expressed in this material are those of the author(s) and do not necessarily reflect the views of the Under Secretary of Defense for Research and Engineering or the National Science Foundation. In addition to the authors listed, we also thank Gregory Allan, Nicholas Pellizzari, Clayton Baumgart, Brian Powers, and Ronald Efromson for their contributions to the project and Mark Silver for his helpful comments.

References

1. T. S. Rose et al., “Optical communications downlink from a 1.5 U cubesat: OCSD program,” *Proc. SPIE* **11180**, 111800J (2019).
2. J. Chang et al., “Body pointing, acquisition and tracking for small satellite laser communication,” *Proc. SPIE* **10910**, 109100P (2019).
3. K. Cahoy et al., “The cubesat laser infrared crosslink mission (click),” *Proc. SPIE* **11180**, 111800Y (2019).
4. H. Takenaka et al., “In-orbit verification of small optical transponder (sota): evaluation of satellite-to-ground laser communication links,” *Proc. SPIE* **9739**, 973903 (2016).
5. E. Clements et al., “Nanosatellite optical downlink experiment: design, simulation, and prototyping,” *Opt. Eng.* **55**(11), 111610 (2016).
6. R. Fields et al., “5.625 gbps bidirectional laser communications measurements between the nfire satellite and an optical ground station,” in *Int. Conf. Space Opt. Syst. and Appl. (ICSOS)*, IEEE, pp. 44–53 (2011).
7. R. Kingsbury, J. Twichell, and S. Palo, “Cobalt optical crosslink transceiver for SWaP-constrained missions,” in *CubeSat Dev. Workshop* (2021).
8. J. Albert, “Satellite-mounted light sources as photometric calibration standards for ground-based telescopes,” *Astron. J.* **143**(1), 8 (2011).
9. A. H. Greenaway, “Satellite-borne laser for adaptive optics reference,” *Proc. SPIE* **1494**, 386–393 (1991).
10. A. H. Greenaway and S. E. Clark, “PHAROS: an agile satellite-borne laser guidestar,” *Proc. SPIE* **2120**, 206–210 (1994).
11. W. A. Marlow et al., “Laser-guide-star satellite for ground-based adaptive optics imaging of geosynchronous satellites,” *J. Spacecr. Rockets* **54**(3), 621–639 (2017).
12. K. Cahoy et al., “Space-based laser guide star mission to enable ground and space telescope observations of faint objects,” in *NAS APC White Pap.* (2019).
13. E. L. Shkolnik, “On the verge of an astronomy cubesat revolution,” *Nat. Astron.* **2**(5), 374–378 (2018).
14. J. G. Chen, V. Shah, and L. Liu, “Performance of a u-net-based neural network for predictive adaptive optics,” *Opt. Lett.* **46**(10), 2513–2516 (2021).
15. B. Weeden, P. Cefola, and J. Sankaran, “Global space situational awareness sensors,” in *AMOS Conf.* (2010).
16. C. Bonnal, J.-M. Ruault, and M.-C. Desjean, “Active debris removal: recent progress and current trends,” *Acta Astron.* **85**, 51–60 (2013).
17. C. R. Phipps et al., “Removing orbital debris with lasers,” *Adv. Space Res.* **49**(9), 1283–1300 (2012).
18. D. Murphy, “Atmospheric-turbulence compensation experiments using cooperative beacons,” *Lincoln Lab. J.* **5**(1), 25–44 (1992).
19. J. S. Dierks et al., “Relay mirror experiment overview: a gbl pointing and tracking demonstration,” *Proc. SPIE* **1482**, 146–158 (1991).
20. D. M. Boroson et al., “Overview and results of the lunar laser communication demonstration,” *Proc. SPIE* **8971**, 89710S (2014).

21. E. S. Douglas et al., “Laser guide star for large segmented-aperture space telescopes. i. implications for terrestrial exoplanet detection and observatory stability,” *Astron. J.* **157**(1), 36 (2019).
22. A. Cunningham and R. Legge, “Overview of the agile microsat,” in *IEEE Aerosp. Conf. (50100)*, IEEE, pp. 1–6 (2021).
23. <https://www.spervis.oma.be>
24. A. Thieu and L. Liu, “On-orbit risk mitigation for a 1/2-u laser guidestar payload,” in *Int. Conf. Space Opt. Syst. and Appl. – ICSOS 2022*, Institute of Electrical and Electronics Engineers (2022).
25. Blue Canyon Technologies, “BCT datasheet components ACS” (2020).

Ariel Sandberg is a lead assembly, integration, and test engineer for spacecraft at MIT Lincoln Laboratory. She has contributed to risk reduction, build, and integration activities for a variety of public and defense space missions, from rapid development CubeSat missions to novel GEO asset payloads. Previously, she served as a solar array engineer for SpaceX’s Starlink mega-constellation. She is passionate about leveraging lessons learned from industry to accelerate development cadence of space assets.

Albert Thieu is a first lieutenant in the United States Air Force. From 2020 to 2022, he worked as a military fellow at MIT Lincoln Laboratory while receiving his MS in aeronautics and astronautics from MIT (’22). He received his BS in astronautic engineering from the United States Air Force Academy (’20). He is currently a student at Euro-NATO Joint Jet Pilot Training at Sheppard Air Force Base, Texas.

Anil Mankame is a member of technical staff at Rapid Prototyping Group in MIT Lincoln Laboratory. His 20 plus years of experience include mechanical systems design, mechanisms, automation, controls, and vibrations. Currently, he has been supporting programs at various roles in space systems, UAVs, and hypersonics. He received his PhD in mechanical engineering from the University of Rhode Island (1997).

Zachary Palmer: Biography is not available.

Joel Kiers is an electrical engineering graduate of Taylor University (BS, ’13). His areas of expertise include embedded software and firmware for defense and aerospace applications. He is employed by Raytheon Missile Systems in Tucson, Arizona, for two years prior to working for 3 years at MIT Lincoln Laboratory as an Associate Staff member in the Advanced Capabilities and Technologies group. Currently working as a senior FPGA developer for The MITRE Corporation in Bedford, Massachusetts.

Mark Wilder is an optical engineer and has been a technical staff member at MIT Lincoln Laboratory since 2016. He is currently working on space-borne imaging and laser communication systems. He received his BS in optics from the University of Rochester (’85), MS in electrooptics from Tufts University (’92), and an MBA from Babson College (’12).

Lulu Liu is a member of technical staff at MIT Lincoln Laboratory specializing in experimental optical physics. Her work is currently focused in the areas of adaptive optics (AO) and nanoscale optics. She received her PhD in applied physics from Harvard University (’16) and her BS in physics from MIT (’09).